

On the Theory and Computation of Surface Tension: The Elimination of Parasitic Currents through Energy Conservation in the Second-Gradient Method

Didier Jamet, David Torres, and J. U. Brackbill

Commissariat à l'Energie Atomique, Grenoble, France; and Theoretical Division, Los Alamos National Laboratory, Los Alamos, New Mexico 87545

E-mail: jamet@cea.fr, dtorres@lanl.gov, and jub@lanl.gov

Received October 12, 2001; revised June 20, 2002

Errors in the computation of fluid flows with surface tension are examined. These errors cause large parasitic flows when the capillary number is large and have often been attributed to truncation error in underresolved interfacial regions. A study using the second-gradient method reveals that when truncation error is eliminated in the computation of energy exchanges between surface and kinetic energies so that energy is strictly conserved, the parasitic currents are reduced to round-off. The results are based on general thermodynamic arguments and can be used to guide improvements in other methods, such as the continuum-surface-force (CSF) method, which is commonly used with the volume-of-fluid (VOF) method. © 2002 Elsevier Science (USA)

1. INTRODUCTION

The accurate computation of surface tension is a critical component of any model for the dynamics of a fluid interface. Molecular forces are responsible for placing liquid surfaces in tension. Their action occurs over scales that are unresolved in ordinary fluid dynamics calculations, and the resulting tension is incorporated in Laplace's formula as a surface stress condition [12]. This computationally inconvenient description of the effect of surface tension is replaced in some recent models by an equivalent volume force, which acts on scale lengths comparable to the grid spacing rather than the thickness of the interface [2, 11, 18]. This is a familiar approach in fluid dynamics, where, as in shocks, essential physics occurs on unresolved scales. Traditional computational fluid dynamics methods, such as front-tracking, level-set, and front-capturing methods, seek to integrate

the contributions of interfaces into more general fluid dynamics problems without resolving the interfacial region. Other models, like phase-field and second-gradient methods, include the excess energy contributed by the interfacial region [10, 13]. The latter methods result in equations that are thermodynamically consistent but require that the interfacial region be resolved by the computation mesh [8].

The challenge that seems to be peculiar to surface tension modeling for fluid/fluid interfaces is the presence of parasitic currents [11]. These are described as a “small amplitude velocity field due to a slight unbalance between stresses in the interfacial region” [11, p. 142]. The parasitic currents seem to occur despite differences in methods, such as SURFER and continuum-surface-force methods (CSF) [2], used with the volume-of-fluid (VOF) method, the front-tracking method [18], and the second-gradient method [9]. The source of parasitic currents seems obvious for VOF methods. The interfacial regions are made as thin as possible and, consequently, are usually underresolved. In the case of CSF, the curvature of the surface is needed, and it is calculated by differentiating the density twice. This contributes large truncation errors when the interfacial region is one cell wide. However, the second-gradient method resolves the interfacial region and parasitic currents are still present. Reducing their magnitude by highly resolving the interfacial region is too costly a solution for practical purposes.

Many of the remedies that are proposed for parasitic currents are aimed at reducing or counteracting the truncation error. In CSF, for example, the surface curvature is calculated from a smoothed density gradient while an approximate delta function, which localizes the surface tension force to the interfacial region, uses an unsmoothed density [2]. Popinet and Zaleski propose a pressure-gradient correction [14]. Torres and Brackbill experiment with a projection method [17]. Lafaurie *et al.* develop a momentum-conserving form of the volume force [11]. These remedies have had some success in reducing parasitic currents, but not in eliminating them.

Jacqmin suggests another line of investigation entirely [8]. He remarks, “It is easy to generate phase-field numerical implementations that are dissipative of energy, and that therefore are free of parasitic flows” [8, p. 98]. (In this context, dissipative means that the total energy of the system decreases with time.) One might be tempted to discount the applicability of this statement to CFD methods, because experience suggests CFD methods are never entirely free of parasitic currents, even with large viscous dissipation. Lafaurie *et al.* characterize the parasitic flows by the capillary number, C_a , the ratio of viscous to surface tension forces [11]. C_a varies from one method to another, $10^{-4} < C_a < 10^{-2}$, and for any given method the parasitic flow varies inversely with the viscosity but is never absent. Nevertheless, the presence of parasitic currents in calculations with the second-gradient method motivate our attempt to understand what, in addition to dissipation, is required for their elimination. While we use the second-gradient method for this investigation, there is some reason to hope that it may benefit CFD methods as well, for Jacqmin shows that CSF is equivalent to his formulation of the phase-field method with a particular scaling [8].

In Section 2, we briefly review the second-gradient method, derive an energy integral and show that it is a constant of the motion, and examine the validity of the resulting description of surface tension. In Section 3, we analyze the necessary conditions to reach equilibrium, develop numerical discretizations that respect these conditions, and test them numerically. Finally, we present computations which reveal, with some precision, that strict energy conservation is required to eliminate parasitic flow.

2. VARIATIONAL FORM OF A GENERAL SECOND-GRADIENT METHOD

Diffuse interface methods model interfaces as continuous transitions across which an order parameter varies rapidly but continuously. In these methods, the energy of the system depends on both the order parameter and its gradient [1]. This allows the interface to have a finite thickness and an energy, the latter of which is interpreted as a surface tension. Indeed, it is possible to deduce the equilibrium order parameter distribution. In the case of the Cahn–Hilliard theory, which described interfaces separating two different fluids, the order parameter is the mass concentration of one of the components of the system. When modeling the solidification of single-component materials, the so-called phase field is used to characterize the phases. For liquid–vapor interfaces, the second-gradient method, which is based on van der Waals’ theory of capillarity, can be used to model flows with phase change [9]. The order parameter for the second-gradient method is the mass density.

The term “second-gradient” reflects the origin of the method in the solid dynamics literature [4]. Second-gradient theory describes both the mechanical and thermodynamical behavior of systems in which an interface is present [5]. With van der Waals’ theory of capillarity, the velocity field is twice differentiable, and therefore the virtual power depends not only on $\nabla \mathbf{v}$ but also on $\nabla \nabla \mathbf{v}$ [7]. Within the framework of the second-gradient theory, it is possible to deduce the ODE governing the equilibrium mass density distribution from the force balance law [10].

2.1. Momentum Balance Equation

A fluid endowed with internal capillarity is defined as a fluid whose energy depends not only on its density and temperature but also on its density gradient. Such a fluid is also called a van der Waals or Cahn–Hilliard fluid or a fluid of second grade. To simplify the analysis, we restrict our study to isothermal cases.

It is known that the second-gradient theory allows a Hamiltonian formulation for the equations of motion of fluid with internal capillarity (see [3], for instance). If we simplify the problem by considering isothermal flows, the Lagrangean \mathcal{L} is then defined as

$$\mathcal{L} \equiv \rho \left(\frac{\mathbf{v}^2}{2} - \Omega - e_f(\rho, \nabla \rho) \right),$$

where e_f is the Helmholtz free energy per unit mass, Ω is the potential due to body forces, and \mathbf{v} is the velocity.

The equations of motion are derived by minimizing the Hamiltonian action a ,

$$a = \int_{t_1}^{t_2} \int_D \mathcal{L} dV dt.$$

If one neglects the boundary terms coming from integration by parts in space and time, minimizing the action yields the momentum balance equation,

$$\rho \frac{d\mathbf{v}}{dt} = -\nabla(P - \rho \nabla \cdot \Phi) - \rho \nabla \Omega - \nabla \cdot (\Phi \otimes \nabla \rho), \quad (1)$$

where P and Φ , a vector, are defined by

$$\Phi = \rho \left(\frac{\partial e_f}{\partial \nabla \rho} \right)_\rho, \quad (2)$$

$$P = \rho^2 \left(\frac{\partial e_f}{\partial \rho} \right)_{\nabla \rho}. \quad (3)$$

2.2. Energy Conservation

The total energy \mathcal{E} is the sum of the free, potential, and kinetic energies:

$$\mathcal{E} \equiv \int_D \rho \left(\frac{\mathbf{v}^2}{2} + e_f(\rho, \nabla \rho) + \Omega \right) dV.$$

We show that this energy, except for boundary contributions, is a constant of the motion. We assume the potential, Ω , is constant in time. Although we also assume the fluid velocity is zero on the boundary of the domain D , we integrate over a Lagrangean domain D whose boundary moves with the local fluid velocity, so that

$$\frac{d\mathcal{E}}{dt} = \int_D \rho \left(\frac{de_f}{dt} + \mathbf{v} \cdot \frac{d\mathbf{v}}{dt} \right) dV. \quad (4)$$

The time derivative of the kinetic energy is computed by forming the inner product of \mathbf{v} with the momentum equation, (1):

$$\rho \mathbf{v} \cdot \frac{d\mathbf{v}}{dt} = -\mathbf{v} \cdot [\nabla P - \nabla(\rho \nabla \cdot \boldsymbol{\Phi}) + \nabla \cdot (\boldsymbol{\Phi} \otimes \nabla \rho) + \rho \nabla \Omega]. \quad (5)$$

The free energy is a function of ρ and $\nabla \rho$, and its time derivative is

$$\frac{de_f}{dt} = \frac{\partial e_f}{\partial \rho} \frac{d\rho}{dt} + \frac{\partial e_f}{\partial \nabla \rho} \cdot \frac{d\nabla \rho}{dt}. \quad (6)$$

From the mass balance equation,

$$\frac{d\rho}{dt} = -\rho \nabla \cdot \mathbf{v}, \quad (7)$$

one readily derives

$$\frac{d\nabla \rho}{dt} = -\nabla(\rho \nabla \cdot \mathbf{v}) - \nabla \mathbf{v} \cdot \nabla \rho. \quad (8)$$

Substituting from Eqs. 2 and 3, one finds

$$\rho \frac{de_f}{dt} = -\boldsymbol{\Phi} \cdot (\rho \nabla \cdot \mathbf{v}) - \boldsymbol{\Phi} \cdot (\nabla \mathbf{v} \cdot \nabla \rho) - P(\nabla \cdot \mathbf{v}). \quad (9)$$

When one combines the kinetic and free energy terms and integrates by parts, the only terms that survive are contributions to $\frac{d\mathcal{E}}{dt}$ from the boundary,

$$\frac{d\mathcal{E}}{dt} = \int_{\partial D} -\hat{\mathbf{n}} \cdot (\mathbf{v}P + \boldsymbol{\Phi} \nabla \cdot (\rho \mathbf{v}) - \rho \mathbf{v}(\nabla \cdot \boldsymbol{\Phi} + \Omega)) dS, \quad (10)$$

where ∂D is the boundary of domain D and $\hat{\mathbf{n}}$ is the outward-directed normal at the surface.

If total energy is to be conserved, note that not only must $\mathbf{v} \cdot \hat{\mathbf{n}} = \mathbf{0}$ be true, but also $\boldsymbol{\Phi} \cdot \hat{\mathbf{n}} = \mathbf{0}$ must be satisfied. The latter condition is related to the moving contact line on the boundaries

(e.g., [16]), which is beyond the scope of this study, in which we do not consider interfaces in contact with boundaries. We also assume that \mathbf{v} is zero on the boundary and thus that energy is a constant of the motion.

3. ELIMINATION OF THE PARASITIC CURRENTS FOR VAN DER WAALS' FLUIDS

Van der Waals first introduced the notion of a fluid endowed with internal capillarity more than a century ago. Originally, the model was intended to describe an interface between the vapor phase and the liquid phase of a pure fluid at equilibrium. The model was purely thermodynamic and therefore the fluid had to be considered compressible (as is a classic fluid for which the specific volume can change). In this thermodynamic model the expression for the Helmholtz free energy per unit volume is

$$E_f(\rho, \nabla\rho) = E_f^0(\rho) + \frac{\lambda}{2}(\nabla\rho)^2,$$

where λ is a constant.

A van der Waals fluid is therefore a particular fluid endowed with internal capillarity. However, this particular expression can be justified using a mean field theory (e.g., [15]).

Moreover, recently Jamet *et al.* [9] showed that such a thermodynamic model could be used as a numerical method to simulate liquid–vapor flows with phase change. However, like any other front-tracking or front-capturing method that uses a fixed grid, parasitic currents were observed when an inclusion should have been at equilibrium. The issue of the existence of parasitic currents dates back to the introduction of surface tension as a continuous force by Brackbill *et al.* [2] and has been investigated by several authors (e.g., [11, 14, 17]). In the best cases, the intensity of the parasitic currents is reduced but not eliminated. In this section, we show how the parasitic currents can be reduced to round-off with the second-gradient method, provided energy transfers between kinetic and surface energies are correctly calculated in the discretized equations.

3.1. Equilibrium State

In Section A.3, it is shown that the equilibrium state of a fluid endowed with internal capillarity is such that its general chemical potential is uniform (A.4). In the particular case of a van der Waals fluid (and for no-slip boundary conditions), this condition reads

$$\mu^0 - \nabla \cdot (\lambda \nabla \rho) = \mu^{eq}, \quad (11)$$

where $\mu^0 \triangleq dE_f^0/d\rho$.

This equilibrium condition should be recovered for the discretized variables.

3.2. How a Closed System Reaches Its Equilibrium State

In Section A.3, it is shown that for a closed system with no-slip boundary conditions, the velocity field should be zero everywhere in the domain. This analysis is based purely on thermodynamic arguments. Now, for an isothermal system, the only information available during a numerical simulation comes from the mass and momentum balance equations and not the second law of thermodynamics. Therefore, we have to check that the mass and momentum balance equations are indeed such that the total free energy of a closed system

decreases with time to reach a minimum, which is characteristic of its equilibrium state. In Section 2.2, it is shown that for a perfect fluid endowed with internal capillarity and *a fortiori* for a van der Waals fluid, the total energy of the system is conserved. In order to make the analysis clearer and to derive a numerical scheme, the time variation of the total energy is derived for a dissipative van der Waals fluid.

3.2.1. Balance Equations

In Section 2, the general form of the momentum balance equation is derived for a fluid endowed with internal capillarity by minimizing the action. In the particular case of a van der Waals fluid, the expression for the pressure P takes the form

$$P = P^0 - \frac{\lambda}{2}(\nabla\rho)^2,$$

where P^0 is the classical thermodynamic pressure defined by

$$P^0(\rho) \doteq \rho \frac{dE_f^0}{d\rho} - E_f^0.$$

Hamilton's principle allows the determination of the equations of motion of perfect fluids. In order to account for dissipative effects, a viscous tensor $\boldsymbol{\tau}^D$ is introduced. Viscosity exerts a dissipative stress such that $(\boldsymbol{\tau}^D : \nabla\mathbf{v}) \geq \mathbf{0}$ in order that the second law of thermodynamics is satisfied. (A Newtonian form can be used.) The equations of motion of a van der Waals fluid therefore read

$$\frac{\partial\rho}{\partial t} + \nabla \cdot (\rho\mathbf{v}) = \mathbf{0}, \quad (12)$$

$$\frac{\partial(\rho\mathbf{v})}{\partial t} + \nabla \cdot (\rho\mathbf{v}\mathbf{v}) = \mathbf{f} + \nabla \cdot \boldsymbol{\tau}, \quad (13)$$

$$\boldsymbol{\tau} \doteq \left[-P^0 + \lambda \left(\frac{1}{2}(\nabla\rho)^2 + \rho \nabla \cdot (\nabla\rho) \right) \right] \mathbf{I} - \lambda \nabla\rho \otimes \nabla\rho + \boldsymbol{\tau}^D, \quad (14)$$

where \mathbf{I} is the unit tensor of rank 2 and \mathbf{f} is a body force such as gravity, for instance, which will be neglected from now on.

The particular form (14) of the stress tensor valid for a van der Waals fluid accounts for surface tension as a continuous force, as presented in Section A.2. The expression for the surface tension *at equilibrium* is found to be

$$\sigma = \int_{-\infty}^{+\infty} \lambda \left(\frac{d\rho}{dz} \right)^2 dz,$$

where z is the coordinate normal to the interface.

3.2.2. Time Evolution of the Total Free Energy of an Isothermal System

To know whether a closed system will reach an equilibrium state characterized by a minimum of its free energy, we must calculate the evolution of the total energy,

$$\frac{d}{dt} \int_D E_{tot} dV,$$

where

$$E_{tot} \hat{=} E_f^0(\rho) + \frac{\lambda}{2}(\nabla\rho)^2 + \rho \frac{\mathbf{v}^2}{2}$$

is the total volumetric free energy of the fluid.

Using the thermodynamic relations

$$\mu^0 = \left(\frac{\partial E_f^0}{\partial \rho} \right)_T, \quad (15)$$

$$\left(\frac{\partial P^0}{\partial \rho} \right)_T = \rho \left(\frac{\partial \mu^0}{\partial \rho} \right)_T \Rightarrow \nabla P^0 = \rho \nabla \mu^0 \quad (16)$$

and integrating by parts, it can be shown that

$$\frac{d}{dt} \int_D E_{tot} dV = - \int_D (\boldsymbol{\tau}^D : \nabla \mathbf{v}) dV + \int_{\partial D} \mathbf{n} \cdot \boldsymbol{\Phi}_E d\mathbf{S}, \quad (17)$$

where μ^0 is the chemical potential and $\boldsymbol{\Phi}_E$ is the total free energy flux at the boundary (which is zero for no-slip boundary conditions).

Since $(\boldsymbol{\tau}^D : \nabla \mathbf{v})$ is never negative, the total free energy of a closed system filled with a van der Waals fluid decreases due to viscous effects.

3.3. Numerical Equilibrium

In order to recover a physical equilibrium state (in particular without parasitic currents), the discretized form of the mass and momentum balance equations (12) and (13) should be such that the total discretized free energy of a system decreases (17).

A close analysis of the proof of the relation (17) shows that besides the relations (15) and (16), the relations

$$\nabla \cdot (\nabla \rho \otimes \nabla \rho) = \nabla \rho \nabla \cdot (\nabla \rho) + \frac{1}{2} \nabla [(\nabla \rho)^2], \quad (18)$$

$$\nabla \cdot (a\mathbf{B}) = \nabla a \cdot \mathbf{B} + a \nabla \cdot \mathbf{B}, \quad (19)$$

where a is any scalar and \mathbf{B} is any vector, must also be satisfied.

Since these relations are necessary to prove that, starting from the mass and momentum balance equations, the total free energy of the system decreases with time, these relations should also be satisfied for the discretized variables and discretized differential operators to reach a numerical equilibrium similar to the physical equilibrium state, i.e., without parasitic currents. The issue is thus to find a spatial numerical scheme that satisfies the discretized form of Eqs. (16), (18), and (19). This issue is addressed in the following.

3.3.1. Spatial Numerical Scheme

For the sake of simplicity, we use a regular MAC grid on which the scalars are stored at the cell centers (i, j) (in two dimensions) and the horizontal and vertical components of

vectors are stored at the cell edges $((i + \frac{1}{2}, j)$ and $(i, j + \frac{1}{2})$, respectively). The discretized gradient operator is defined as

$$\begin{aligned} (\nabla a)_{i+\frac{1}{2},j}^x &\hat{=} \frac{a_{i+1,j} - a_{i,j}}{\Delta x}, \\ (\nabla a)_{i,j+\frac{1}{2}}^y &\hat{=} \frac{a_{i,j+1} - a_{i,j}}{\Delta y}, \end{aligned} \quad (20)$$

where Δx and Δy are the constant grid spacing in the horizontal and vertical directions, respectively.

Given the definition (20), the following interpolations must be used, so that the discretized form of relation (19) may be satisfied:

$$\begin{aligned} a_{i+\frac{1}{2},j} &\hat{=} \frac{a_{i+1,j} + a_{i,j}}{2}, \\ a_{i,j+\frac{1}{2}} &\hat{=} \frac{a_{i,j+1} + a_{i,j}}{2}. \end{aligned} \quad (21)$$

Similarly, the discretized divergence of vector and inner products of two vectors are defined as

$$(\nabla \cdot \mathbf{B})_{i,j} \hat{=} \frac{\mathbf{B}_{i+\frac{1}{2},j}^x - \mathbf{B}_{i-\frac{1}{2},j}^x}{\Delta x} + \frac{\mathbf{B}_{i,j+\frac{1}{2}}^y - \mathbf{B}_{i,j-\frac{1}{2}}^y}{\Delta y}, \quad (22)$$

$$(\mathbf{A} \cdot \mathbf{B})_{i,j} \equiv \frac{\mathbf{A}_{i+\frac{1}{2},j}^x \mathbf{B}_{i+\frac{1}{2},j}^x + \mathbf{A}_{i-\frac{1}{2},j}^x \mathbf{B}_{i-\frac{1}{2},j}^x}{2} + \frac{\mathbf{A}_{i,j+\frac{1}{2}}^y \mathbf{B}_{i,j+\frac{1}{2}}^y + \mathbf{A}_{i,j-\frac{1}{2}}^y \mathbf{B}_{i,j-\frac{1}{2}}^y}{2}. \quad (23)$$

Relation (18) is satisfied at the discretized level if the following numerical scheme is used with $\Delta x = \Delta y$:

$$\begin{aligned} [(\nabla \rho)^2]_{i,j} &\hat{=} \frac{[(\nabla \rho)_{i+\frac{1}{2},j}^x]^2 + [(\nabla \rho)_{i-\frac{1}{2},j}^x]^2}{2} + \frac{[(\nabla \rho)_{i,j+\frac{1}{2}}^y]^2 + [(\nabla \rho)_{i,j-\frac{1}{2}}^y]^2}{2}, \\ (\nabla \rho \otimes \nabla \rho)_{i,j}^{xx} &\hat{=} \left[\frac{(\nabla \rho)_{i+\frac{1}{2},j}^x + (\nabla \rho)_{i-\frac{1}{2},j}^x}{2} \right]^2, \\ (\nabla \rho \otimes \nabla \rho)_{i,j}^{yy} &\hat{=} \left[\frac{(\nabla \rho)_{i,j+\frac{1}{2}}^y + (\nabla \rho)_{i,j-\frac{1}{2}}^y}{2} \right]^2, \\ (\nabla \rho \otimes \nabla \rho)_{i+\frac{1}{2},j+\frac{1}{2}}^{xy} &\hat{=} \left[\frac{(\nabla \rho)_{i+\frac{1}{2},j}^x + (\nabla \rho)_{i+\frac{1}{2},j+1}^x}{2} \right] \left[\frac{(\nabla \rho)_{i,j+\frac{1}{2}}^y + (\nabla \rho)_{i+1,j+\frac{1}{2}}^y}{2} \right]. \end{aligned}$$

It must be noted that the discretized value of the scalar $(\nabla \rho)^2$ is obtained by calculating *the mean value of the square of the gradient*, whereas the discretized value of the components of the tensor $(\nabla \rho \otimes \nabla \rho)$ are obtained by calculating *the square of the mean value of the gradient*.

Given our particular choice of the discretized differential operators (20) and (22), the relations (18) and (19) are satisfied at the discrete level. The resulting momentum balance

equation in conservative form is

$$\left[\frac{\partial(\rho \mathbf{v})}{\partial t} + \nabla \cdot (\rho \mathbf{v} \mathbf{v}) = -\nabla P^0 + \rho \nabla(\nabla \cdot (\lambda \nabla \rho)) + \nabla \cdot \boldsymbol{\tau}^D \right]_{i+\frac{1}{2},j}^x, \quad (24)$$

$$\left[\frac{\partial(\rho \mathbf{v})}{\partial t} + \nabla \cdot (\rho \mathbf{v} \mathbf{v}) = -\nabla P^0 + \rho \nabla(\nabla \cdot (\lambda \nabla \rho)) + \nabla \cdot \boldsymbol{\tau}^D \right]_{i,j+\frac{1}{2}}^y.$$

The mass balance equation is differenced:

$$\left(\frac{\partial \rho}{\partial t} \right)_{i,j} = \frac{(\rho \mathbf{v})_{i+\frac{1}{2},j} - (\rho \mathbf{v})_{i-\frac{1}{2},j}}{\Delta x} + \frac{(\rho \mathbf{v})_{i,j+\frac{1}{2}} - (\rho \mathbf{v})_{i,j-\frac{1}{2}}}{\Delta y}. \quad (25)$$

Note that the actual variable stored on the cell edges is the momentum $\rho \mathbf{v}$ and not the velocity \mathbf{v} .

A numerical test of this discretization, the results for which are shown in Figs. 1 and 2, does not confirm that an equilibrium is reached. In Fig. 1, the mean kinetic energy, labeled “conservative,” is shown for a cylindrical drop on a 51 by 51 grid. The initial conditions correspond to an approximation of the density field at equilibrium; i.e., curvature effects are neglected and a density profile of a *plane* interface at equilibrium is used. The interface is resolved by about four grid points: $h \simeq 4\Delta x$. In the computation the mean kinetic energy, which rises abruptly at $t=0$ because of numerical truncation errors in the initial force balance, decreases exponentially thereafter by five orders of magnitude, and then remains constant for the remainder of the calculation. A velocity vector plot, Fig. 2 (left), indicates that the flow at the end of the calculation is organized into eight eddies with centers lying

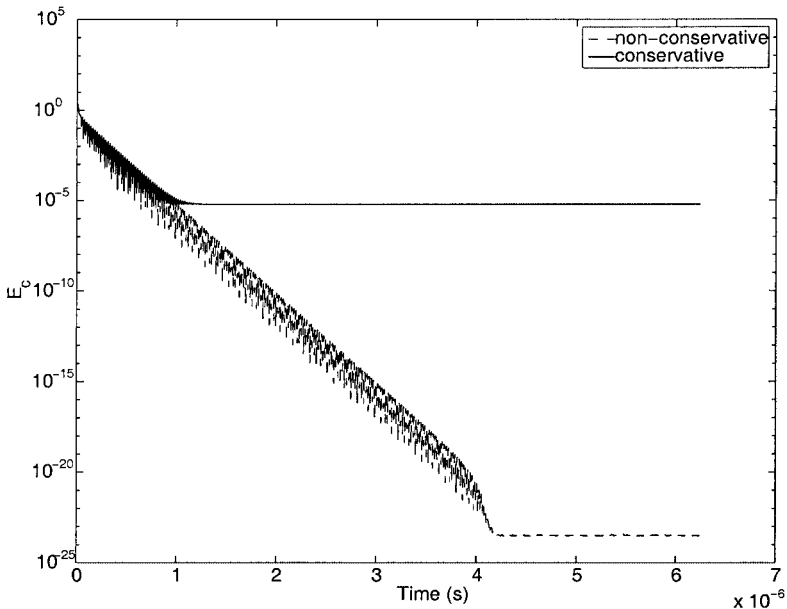


FIG. 1. Time evolution of the mean kinetic energy is plotted for a conservative and a nonconservative form of the momentum balance equation for a 51 by 51 grid.

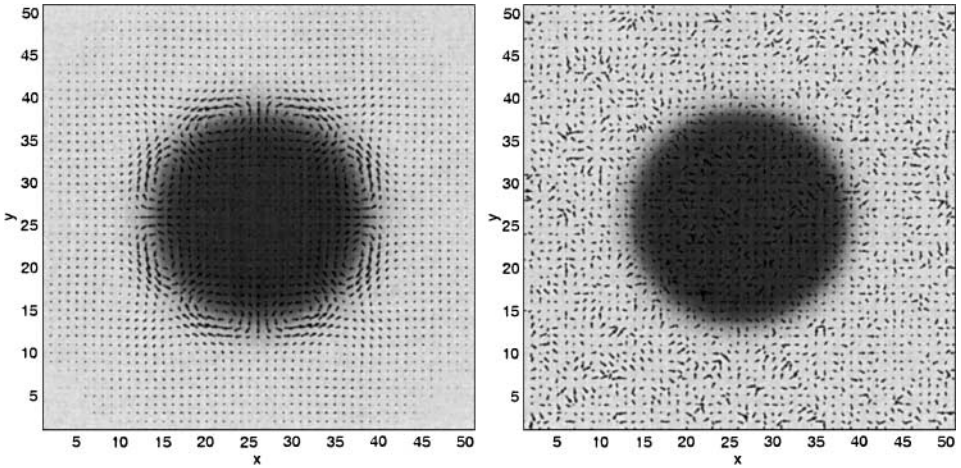


FIG. 2. Velocity fields are shown for a momentum conservative (left) and energy conservative (right) form of the momentum balance equation. The momentum conservative form results in velocity values 10 orders of magnitude higher than the energy conservative form and in organized flow patterns typical of parasitic currents. Values of the density field are indicated by shades of gray. Dark gray represents low-density values.

on the interface. The eddies are approximately time stationary and correspond closely to descriptions of the parasitic currents observed with other methods.

The results are inconsistent with the proof that an equilibrium exists with the second-gradient method. The time stationary flow in Fig. 2 (left) results from a balance between dissipation and residual, unbalanced forces due to a lack of equilibrium. It is shown in Section 3.2.2 that the thermodynamic relation (16) is also necessary to prove that the free energy decreases in time. The issue of its validity for discretized variables and differential operators is addressed in the next section.

3.3.2. Discretization of the Pressure Term for Thermodynamic Consistency

Since the pressure P^0 and the chemical potential μ^0 are functions of the density, these quantities are known at the nodes (i, j) . Given the definitions (20) and (21), the discretized form of the relation (16) should be

$$\begin{aligned} \frac{P_{i+1,j}^0 - P_{i,j}^0}{\Delta x} &= \frac{\rho_{i+1,j} + \rho_{i,j}}{2} \frac{\mu_{i+1,j}^0 - \mu_{i,j}^0}{\Delta x}, \\ \frac{P_{i,j+1}^0 - P_{i,j}^0}{\Delta y} &= \frac{\rho_{i,j+1} + \rho_{i,j}}{2} \frac{\mu_{i,j+1}^0 - \mu_{i,j}^0}{\Delta y}. \end{aligned} \tag{26}$$

Making Taylor expansions of the pressure and of the chemical potential up to an order of 3, it is found that

$$\begin{aligned} \left(\frac{\partial P^0}{\partial x}\right)_{i+1/2,j} - \rho_{i+1/2,j} \left(\frac{\partial \mu^0}{\partial x}\right)_{i+1/2,j} &= \left(\frac{\partial^2 \mu^0}{\partial \rho^2}\right)_{i+1/2,j} \left(\frac{\partial \rho}{\partial x}\right)_{i+1/2,j}^3 \frac{\Delta x^2}{12}, \\ \left(\frac{\partial P^0}{\partial y}\right)_{i,j+1/2} - \rho_{i,j+1/2} \left(\frac{\partial \mu^0}{\partial y}\right)_{i,j+1/2} &= \left(\frac{\partial^2 \mu^0}{\partial \rho^2}\right)_{i,j+1/2} \left(\frac{\partial \rho}{\partial y}\right)_{i,j+1/2}^3 \frac{\Delta y^2}{12}. \end{aligned} \tag{27}$$

Relations (27) show that *the relations (26) are not satisfied exactly and that a quadratic truncation error is introduced proportional to $(\partial^2 \mu^0 / \partial \rho^2)$* . Computations show that, when the mesh is doubled using the conservative form of the momentum balance equation, the maximum velocity of the flow decreases by a factor of 4, whereas the mean kinetic energy of the flow decreases by a factor of 15 ($\simeq 4^2$).

Since the thermodynamic relation (16) is necessary for the free energy to decrease and since it is not satisfied for the discretized variables and differential operators chosen, we write the momentum balance equation in a nonconservative form, replacing the pressure term ∇P^0 with $(\rho \nabla \mu^0)$. The relation (26) is therefore imposed.

Again using the discretized differential operators (20) and (22), the relations (18) and (19) are satisfied at the discrete level. Since we write the momentum balance equation in a nonconservative form, the momentum balance equation that is actually solved is

$$\left[\frac{\partial(\rho \mathbf{v})}{\partial t} + \nabla \cdot (\rho \mathbf{v} \mathbf{v}) = -\rho \nabla[\mu^0 - \nabla \cdot (\lambda \nabla \rho)] + \nabla \cdot \boldsymbol{\tau}^{\mathbf{D}} \right]_{i+\frac{1}{2},j}^x, \quad (28)$$

$$\left[\frac{\partial(\rho \mathbf{v})}{\partial t} + \nabla \cdot (\rho \mathbf{v} \mathbf{v}) = -\rho \nabla[\mu^0 - \nabla \cdot (\lambda \nabla \rho)] + \nabla \cdot \boldsymbol{\tau}^{\mathbf{D}} \right]_{i,j+\frac{1}{2}}^y.$$

The mass balance equation (25) is unchanged.

A numerical test of this new scheme, labeled “non-conservative” in Fig. 1, shows that the mean kinetic energy decreases exponentially by 23 orders of magnitude from its maximum value! Further, there are no organized flow structures in the velocity vector plot (Fig. 2, right). The magnitude of the velocity is not only more than 10 orders of magnitude smaller than in the momentum conservative case, but also its direction appears to be random. One may reasonably argue that the numerical computations result in a numerical equilibrium to which the contribution of truncation error is negligible.

These results show that *the parasitic currents are eliminated* by using a nonconservative form of the pressure-gradient term in the momentum balance equation. Evidently, the most important feature of the system of the discretized equations of motion of the fluid is not that the momentum balance equation is written in a conservative form but that the energy transfer between the kinetic energy and the surface tension energy is correctly accounted for in the discretized equations. In view of the discussion in the following section, we refer to the resulting scheme as the *energy conserving discretization*. Note that these results are very similar to those obtained by Jacqmin [8], who also had to write the momentum balance equation in a nonconservative form (Eq. (2.9)).

3.3.3. Energy Conservation

Knowing the density $\rho_{i,j}$ from (25) and the momenta $(\rho \mathbf{v})_{i+\frac{1}{2},j}$ and $(\rho \mathbf{v})_{i,j+\frac{1}{2}}$ from (28), we define the velocities as

$$\mathbf{v}_{i+\frac{1}{2},j}^x \triangleq \frac{(\rho \mathbf{v}^x)_{i+\frac{1}{2},j}}{\rho_{i+\frac{1}{2},j}}, \quad (29)$$

$$\mathbf{v}_{i,j+\frac{1}{2}}^y \triangleq \frac{(\rho \mathbf{v}^y)_{i,j+\frac{1}{2}}}{\rho_{i,j+\frac{1}{2}}}.$$

Following Jacqmin's arguments [8], the rate of change of the free energy is given by

$$\sum_{i,j} -[\nabla \cdot (\rho \mathbf{v})]_{i,j} [\mu^0 - \nabla \cdot (\lambda \nabla \rho)]_{i,j}. \quad (30)$$

Multiplying the discretized momentum balance equation (28) by the velocities $\mathbf{v}_{i+\frac{1}{2},j}$ and $\mathbf{v}_{i,j+\frac{1}{2}}$, and summing over all the nodes, the rate of change of the kinetic energy due to the surface tension force is given by

$$\sum_{i,j} \rho_{i+\frac{1}{2},j} \mathbf{v}_{i+\frac{1}{2},j} \cdot \{\nabla [\mu^0 - \nabla \cdot (\lambda \nabla \rho)]\}_{i+\frac{1}{2},j} + \sum_{i,j} \rho_{i,j+\frac{1}{2}} \mathbf{v}_{i,j+\frac{1}{2}} \cdot \{\nabla [\mu^0 - \nabla \cdot (\lambda \nabla \rho)]\}_{i,j+\frac{1}{2}}. \quad (31)$$

Given the definition of the discretized velocity (29) and the property (19) of the discretized gradient and divergence operators, the sum of (30) and (31) is found to be zero. Therefore, the rate of change of the discretized free energy is equal and opposite to that of the kinetic energy due to the surface tension force.

4. CONCLUSIONS

Through a detailed study of the properties of the second-gradient model for surface tension at a fluid–vapor interface, we have sought a deeper understanding of the cause of parasitic flows. We have established that the second-gradient equations are energy conserving, that the minimum energy state is a static equilibrium, and that equilibrium will be achieved in a dynamical calculation if dissipation is supplied by viscous damping.

Parasitic currents were observed in numerical tests with a momentum conserving discretization of the second-gradient equations. However, further analysis of numerical discretizations of the second-gradient equations shows that when the generalized chemical potential, a scalar, which is uniform at equilibrium, is used in the momentum balance equation, exact balance between kinetic and surface energy terms in the energy equation is achieved. Momentum is conserved to truncation error.

With the energy conserving discretization, numerical results show that parasitic currents are eliminated to round-off. That is, under exactly the same conditions as for the momentum conserving discretization, the residual kinetic energy in the energy conserving calculation is reduced by nearly 20 orders of magnitude.

We conclude that the essential requirement for the elimination of parasitic currents is energy conservation. Strict momentum conservation does not appear to be essential. In the case of the second-gradient method, this particularly means that the numerical scheme for the surface tension force and for the mass flux should not be analyzed separately.

APPENDIX: SURFACE TENSION

Surface tension has two, seemingly different, interpretations. Either it is an energy per unit surface area or a force per unit length tangential to the surface. In this section, both interpretations of the surface tension are analyzed.

A.1. Energy per Surface Area

It has been postulated that the volumetric energy of the fluid, $E_f(\rho, \nabla\rho) = \rho e_f(\rho, \nabla\rho)$, depends upon ρ and $\nabla\rho$. In order to go from a three-dimensional description of an interfacial zone to a two-dimensional description of an interface, it is necessary to introduce so-called “excess” quantities (e.g., [6]). These quantities represent the surface properties with which an interface must be endowed in order for the three-dimensional and the two-dimensional descriptions to be equivalent. If surface tension is interpreted as an energy per unit surface area, it must be the excess energy; i.e.,

$$\sigma_E = \int_{-\infty}^{z_i} (E_f(\rho, \nabla\rho) - E_f^v) dz + \int_{z_i}^{+\infty} (E_f(\rho, \nabla\rho) - E_f^l) dz, \quad (\text{A.1})$$

where z is the coordinate normal to the plane interface, z_i is the position of the interface, defined such that the excess density is zero, and E_f^v and E_f^l are the free energies of the vapor and liquid phases, respectively.

A.2. Force per Unit Length

It has been shown that the dependence of the fluid energy on the density gradient introduces an anisotropic tensor into the momentum balance equation (see Eq. (1)). Following [10], the forces on the edges of an element of fluid located within a plane interface at equilibrium are studied.

At equilibrium, the fluid velocity is zero and the z -component of the momentum balance equation (1) reads

$$p_0(z) + \phi_z \left(\frac{d\rho}{dz} \right) = \text{const.},$$

where p_0 is defined by

$$p_0 \equiv P - \rho \frac{d\phi_z}{dz}.$$

The stresses can be decomposed into normal and tangential components.

- The stress parallel to z is

$$\left(p_0 + \phi_z \left(\frac{d\rho}{dz} \right) \right) \mathbf{z} = \text{const.} \times \mathbf{z}.$$

- The stress normal to z and thus tangential to the interface is

$$p_0 \mathbf{x} = \left(\text{const.} - \phi_z \left(\frac{d\rho}{dz} \right) \right) \mathbf{x}.$$

Therefore, the pressure applied in the direction tangential to the interface is lower than the pressure applied in the direction normal to the interface. A tension ($\phi(d\rho/dz)$) is thus applied in the direction tangential to the interface. The surface tension is therefore given by the relation

$$\sigma_F = \int_{-\infty}^{+\infty} \phi_z \left(\frac{d\rho}{dz} \right) dz. \quad (\text{A.2})$$

A.3. Equivalence

The expressions for the surface tension derived from an energy integral and the momentum balance, Eqs. (A.1) and (A.2), respectively, should be the same. In the following, we show that the surface force and the surface energy have the same expression when the interface is at equilibrium. The equilibrium state of a closed system is then such that its total free energy reaches a minimum; i.e.,

$$\delta \int_D \left[E_f(\rho, \nabla \rho) + \rho \frac{\mathbf{v}^2}{2} + L_1 \rho + \mathbf{L}_2 \cdot (\rho \mathbf{v}) + \mathbf{L}_3 \cdot (\mathbf{x} \times \rho \mathbf{v}) \right] dV = 0,$$

where L_1 , \mathbf{L}_2 , and \mathbf{L}_3 are Lagrange multipliers accounting for the constancy of mass, momentum, and angular momentum of the fluid in a closed system.

The expansion of the above variation leads to the equilibrium conditions

$$\mathbf{v} = (\mathbf{L}_2 + \mathbf{L}_3 \times \mathbf{x}) \equiv \mathbf{v}_{eq} + \Omega_{eq} \times \mathbf{x}, \quad (\text{A.3})$$

$$\mu - \frac{\mathbf{v}^2}{2} - \nabla \cdot \boldsymbol{\phi} = L_1 \equiv \mu^{eq}, \quad (\text{A.4})$$

where $\mu \equiv (\partial E_f / \partial \rho)_{\nabla \rho}$ is the chemical potential.

This analysis shows that the equilibrium of a fluid endowed with internal capillarity is such that *its velocity is that of a rigid body and that its generalized chemical potential is constant*. It particularly shows that if the velocity is zero on the boundaries of the system, the velocity field must be zero everywhere. For a plane interface, let us denote $\cdot' = d \cdot / dz$. One has

$$E'_f = \left[\frac{\partial E_f}{\partial \rho} - \left(\frac{\partial E_f}{\partial \rho'} \right)' \right] \rho' + \left(\frac{\partial E_f}{\partial \rho'} \rho' \right)'. \quad (\text{A.5})$$

Equation (A.4) reads

$$\frac{\partial E_f}{\partial \rho} - \left(\frac{\partial E_f}{\partial \rho'} \right)' = \mu^{eq}.$$

At equilibrium, Eq. (A.5) reads

$$E'_f = \mu^{eq} \rho' + \left(\frac{\partial E_f}{\partial \rho'} \rho' \right)'.$$

Integrating this relation from $-\infty$ to z or from z to $+\infty$ leads to

$$E_f - E_f^v = \frac{\partial E_f}{\partial \rho'} \rho' - \mu^{eq}(\rho - \rho_v),$$

$$E_f - E_f^l = \frac{\partial E_f}{\partial \rho'} \rho' - \mu^{eq}(\rho - \rho_l).$$

Accounting for these two relations, relation (A.1) can be transformed and the expression for the surface tension energy reads

$$\sigma_E = \int_{-\infty}^{+\infty} \Phi_z \left(\frac{d\rho}{dz} \right) dz = \sigma_F.$$

This relation shows that, *at equilibrium*, the expressions for the surface tension interpreted as a force per unit length and interpreted as an energy per unit surface area are the same. It must be noted that this result is very general and does not depend on the particular form of the energy $E_f(\rho, \nabla\rho)$. The only requirement is that the differential equation (A.4) has a solution to determine the density profile $\rho(z)$ across the interface.

ACKNOWLEDGMENTS

This research is supported by the Department of Energy under Contract W-7405-ENG-36, by NASA's Microgravity Science and Applications Division, by the Programme Lavoisier of the Ministère des Affaires Etrangères, and by the Département de Thermohydraulique et de Physique of the Commissariat à l'Énergie Atomique.

REFERENCES

1. D. M. Anderson, G. B. McFadden, and A. A. Wheeler, Diffuse-interface methods in fluid mechanics, *Annu. Rev. Fluid Mech.* **30**, 139 (1998).
2. J. U. Brackbill, D. B. Kothe, and C. Zemach, A continuum method for modeling surface tension, *J. Comput. Phys.* **100**, 335 (1992).
3. P. Casal and H. Gouin, Sur les interfaces liquide-vapeur non isothermes, *J. Méc. Théor. Appl.* **7**(6), 689 (1988).
4. P. Casal and H. Gouin, Relation entre l'équation de l'énergie et l'équation du mouvement en théorie de Korteweg de la capillarité, *C. R. Acad. Sci. Paris* **300**, 231 (1985).
5. F. Dell'Isola, H. Gouin, and G. Rotoli, Nucleation of spherical shell-like interfaces by second-gradient theory: Numerical simulations, *Eur. J. Mech. B* **15**, 545 (1996).
6. D. A. Edwards, H. Brenner, and D. T. Wasan, *Interfacial Transport Processes and Rheology* (Butterworth-Heinemann, Stoneham, MA, 1991).
7. R. Gatignol and P. Seppecher, Modélisation of fluid-fluid interfaces with material properties, *J. Theor. Appl. Mech.*, Special Issue, 225 (1986).
8. D. Jacqmin, Calculation of two-phase Navier–Stokes flows using phase field modeling, *J. Comput. Phys.* **155**, 96 (1999).
9. D. Jamet, O. Lebaigue, N. Coutris, and J. M. Delhayé, The second gradient method for the direct numerical simulation of liquid-vapor flows with phase change, *J. Comput. Phys.* **169**, 624 (2001).
10. D. Jamet, O. Lebaigue, and J. M. Delhayé, A numerical description of a liquid-vapor interface based on the second-gradient theory, *Fluid. Mech. Res.* **22**, 1 (1995).
11. B. Lafaurie, C. Nardone, R. Scardovelli, S. Zaleski, and G. Zanetti, Modelling merging and fragmentation in multiphase flows with SURFER, *J. Comput. Phys.* **113**, 134 (1994).
12. L. D. Landau and E. M. Lifshitz, *Fluid Mechanics* (Pergamon, New York, 1959).
13. G. B. McFadden, A. A. Wheeler, R. J. Braun, S. R. Coriell, and R. F. Sekerka, Phase-field models for anisotropic interfaces, *Phys. Rev. E* **48**, 2016 (1993).
14. S. Popinet and S. Zaleski, A front-tracking algorithm for accurate representation of surface tension, *Int. J. Numer. Methods Fluids* **30**, 775 (1999).
15. J. S. Rowlinson and B. Widom, *Molecular Theory of Capillarity* (Oxford Univ. Press, New York, 1982).
16. P. Seppecher, Etude des conditions aux limites en théorie du second gradient: Cas de la capillarité, *C. R. Acad. Sci.* **309**, 497 (1989).
17. D. J. Torres and J. U. Brackbill, The point-set method: Front-tracking without connectivity, *J. Comput. Phys.* **165**, 620 (2000).
18. G. Tryggvason, B. Bunner, A. Esmaeili, N. Al-Rawahi, D. Juric, W. Tauber, J. Han, S. Nas, and Y.-J. Jan, A front-tracking method for computations of multiphase flow, *J. Comput. Phys.* **169**, 708 (2001).